Design and fabrication of effective gradient temperature sensor array based on bilayer SnO$_2$/Pt for gas classification

Nguyen Van Duy[1*], Nguyen Xuan Thai[1], Trinh Minh Ngoc[1], Chu Manh Hung[1], Hugo Nguyen[2], Matteo Tonezzer[3], Nguyen Van Hieu[4], Nguyen Duc Hoa[1*]

[1] International Training Institute for Materials Science (ITIMS), Hanoi University of Science and Technology (HUST), No. 1, Dai Co Viet, Hanoi, Vietnam

[2] Department of Materials Science and Engineering, Uppsala University, Lägerhyddsvägen 1, 751 21, Uppsala, Sweden

[3] IMEM-CNR, Sede di Trento-FBK, Via alla Cascata 56/C, 38123 Povo-Trento, Italy

[4] Faculty of Electrical and Electronic Engineering, Phenikaa University, Yen Nghia, Ha-Dong district, Hanoi, Vietnam

Corresponding authors:
Email: nguyenvanduy@itims.edu.vn (N V Duy); ndhoa@itims.edu.v (N D Hoa)

Abstract:

Classification of different gases is important and it is possible to use different gas sensors for this purpose. Electronic noses, for example, combine separated gas sensors into an array for detecting different gases. However, the use of separated sensors in an array suffers from being bulky, high energy consumption and complex fabrication processes. Generally, gas sensing properties, including gas selectivity, of semiconductor gas sensors are strongly dependent on their working temperature. It is therefore feasible to use a single device composed of identical sensors arranged in a temperature gradient for classification of multiple gases. Herein, we introduce a design for simple fabrication of gas sensor array based on bilayer Pt/SnO_2 for real-time monitoring and classification of multiple gases. The study includes design simulation of the sensor array to find an effective gradient temperature, fabrication of the sensors and test of their performance. The array, composed of five sensors, was fabricated on a glass substrate without the need of backside etching to reduce heat loss. A SnO_2 thin film sensitized with Pt on top deposited by sputtering was used as sensing material. The sensor array was tested against different gases including ethanol, methanol, isopropanol, acetone, ammonia, and hydrogen. Radar plots and principal component analysis were used to visualize the distinction of the tested gases and to enable effective classification.

Keywords: design of sensor array; electronic nose; gradient temperature; gas classification

1. Introduction

Gas sensors have many applications, including air pollution monitoring, gas leakage detection, industrial process optimization and control, and breath analysis [1,2] [3–5]. Resistive metal oxide semiconductor gas sensors have the advantages of being small size, low cost, portability and robustness [1,2]. For example, it was reported that a metal oxide-based gas sensor with extremely low power consumption could be connected to the "Internet of Things" with a tiny chip for disease diagnosis and patient monitoring [6]. However, a single gas sensor device is not capable to selectively recognize different gases in a mixture [1,2] [7]. Electronic noses and/or multiple sensors are important in practical applications, such as food and beverage industry, agriculture and forestry, medicine and healthcare, indoor and outdoor monitoring, military and civilian security [8] [9]. An electronic nose employing 14 conducting polymers based on polyaniline was used to diagnose tuberculosis, where the specificity of the described method was 91% [10]. Zhang et al. [11] used an array of four separated sensors for detection of acetone, benzene, methanol and formaldehyde. Chen et al. [12] used an array of gas sensors together with algorithms employed in artificial olfactory systems to explore their potential applications in disease diagnosis, environmental monitoring and explosive detection. Güntner et al. [13] used an array of four sensors composed of nanostructured sensing films of highly porous SnO_2 doped with Pt, Si, Pd, and Ti, for quantification of breath-relevant formaldehyde levels. Zhang et al. [14] used an array of six commercial sensors and an artificial neural network for detection of mixed indoor hazardous gases. An array of commercial sensors is bulky and consumes much energy [15] [16]. It is well-known that metal oxide gas sensors exhibit different trends in response to various gases at different temperatures depending on the sensing material [17] [18]. Barsan et al. reported that SnO_2 based sensor showed different trends in response to various

gases at different temperatures with an interval of 50 °C. Based on the working principle of the sensors in temperature gradient, several works have been reported on fabrication of electronic noses using a single sensing material [20]. Tonezzer et al. [21] reported the possibility of using response values at different temperatures from a sensor based on Pt-SnO_2 nanowires, to classify benzene, acetone, hydrogen, toluene, and ethanol via machine learning techniques. Another electronic nose that used a single material (SnO_2 nanowires) decorated with different metallic nanoparticles was reported as an effective device for classification of three reducing gases (H_2, CO, and ethylene) [22]. Yet another electronic nose based on ZnO nanowires, ZnO–$ZnAl_2O_4$ core–shell nanowires and ZnO–Zn_2TiO_4 core–shell nanowires operated under UV illumination was reported that it could discriminate CO, O_2, NO_2, and O_3 gases [23]. An array of sensors based on a single SnO_2 nanobelt decorated with Pd nanoparticles could classify ethanol, isopropyl alcohol, toluene and CO [20] using back-side microheaters to create a temperature gradient for the different sensors. The use of the back-side microheaters required complex fabrication processes [26,27] and therefore was not cost effective for the application [24]. Temperature gradient method was known to be simple and cost effective since a single device composed of an array of sensors with the same sensing material could be used for classification of different gases in a gas mixture [25]. Sysoev et al. used two microheaters to obtain a temperature gradient span of 80 K (from 520–600 K) across the chip [25]. However, the small temperature increments between the electrodes, together with the inhomogeneous distribution of the SnO_2 nanowire as sensing material between them, limited the sensor application. Generally, for practical applications, designs of sensor arrays with simple fabrication processes and effective temperature gradient is practically important [28].

1 Here, a sensor array based on a bilayer Pt/SnO$_2$ thin film with effective temperature gradient in

2 the range of 200 to 400 °C is introduced for gas classification. The design of the sensor was

3 iteratively simulated and the fabrication was performed using conventional photolithography thin

4 film deposition and lift-off. ~~The sensor array within the temperature gradient enables the device~~

5 ~~to operate as an electronic nose for gas classification. The advantages of our sensor array include~~

6 ~~small size, rapidity, stability, portability, and robustness.~~

7 **2. Experimental**

8 **2.1 Design of sensor array**

9 To design the sensor array with effective temperature gradient the COMSOL Multiphysics 5.4

10 software (COMSOL Inc., Burlington, MA, USA) was used to simulate the thermal distribution.

11 The design is shown in Figure 1(A), which includes five sensors denoted as S1, S2, S3, S4 and

12 S5. The sensor chip was fabricated on a glass substrate with dimensions of 6×6 mm^2 and

13 thickness of 0.5 mm. The microheater segments were of the same length but different widths,

14 with heat sinks of the same dimensions in between. In simulation, constrains for Joule heating,

15 thermal radiation and heat transfer in solid were applied. The variables were temperature (*T*) and

16 resistance (*R*) or voltage (*V*). The dependency of a microheater resistance on the temperature can

17 be expressed as:

18
$$R = \frac{\rho L}{wt} \qquad (1.1)$$

19
$$\frac{1}{\rho} = \sigma = \frac{\sigma_0}{1+\alpha(T-T_0)} \qquad (1.2)$$

20 Where ρ is the resistivity of the material, σ is the conductivity of the material, *L, w* and *t* are the

21 length, width and thickness of the microheater, respectively, α is the coefficient of heat

22 resistance, ρ_0 is the electrical resistivity at T_0. The mathematical model for the heat transfer is

23 expressed by the equation:

1
$$\delta C_p \frac{\partial T}{\partial t} - \Delta(k\Delta T) = Q \qquad (1.3)$$

2 where δ is density of the microheater material, C_p is its specific heat, k is its coefficient of

3 thermal conductivity and Q is the heat generated by the electric current flowing through the

4 resistive heater. Q is proportional to the square of the current density J, and is called Joule

5 heating:

6
$$Q \propto |J|^2 = \rho|J|^2 = \frac{1}{\sigma}|J|^2 \qquad (1.4)$$

7 or

8
$$Q = \sigma |\nabla V|^2 \qquad (1.5)$$

9 where σ is the conductivity of the microheater and V is the applied voltage.

10 The power consumption of the microheater is calculated by the equation

11
$$P = \frac{V^2}{R} \qquad (1.6)$$

12 The input parameters for the simulation are summarized in Table 1, where Pt was used as

13 material of the microheater. By changing the widths of the microheater segments iteratively

14 design of a sensor array with temperature gradient from 200 °C to 400 °C with an increment of

15 about 50 °C for each sensor was obtained, as shown in Figure 1(B). The simulated sensor

16 configuration and microheater dimensions were then used for the fabrication of the real device.

17

18 **Table 1.** Physical parameters of Pt microheater for simulation

heater	Dielectric	Conductivity	Coefficient of thermal	Heat capacity	Specific	Thermal	Modul	Coefficient

	constant		expansion	constant	weight	conductivity	Young	Poisson
		(S/m)	(1/K)	(J/kg*K)	(kg/m³)	(W/(m*K))	(Pa)	
Pt	1.27E-06 (0.08)-0.6	8.90E+06	8.80E-06	133	21450	71.6	1.68E+11	0.38
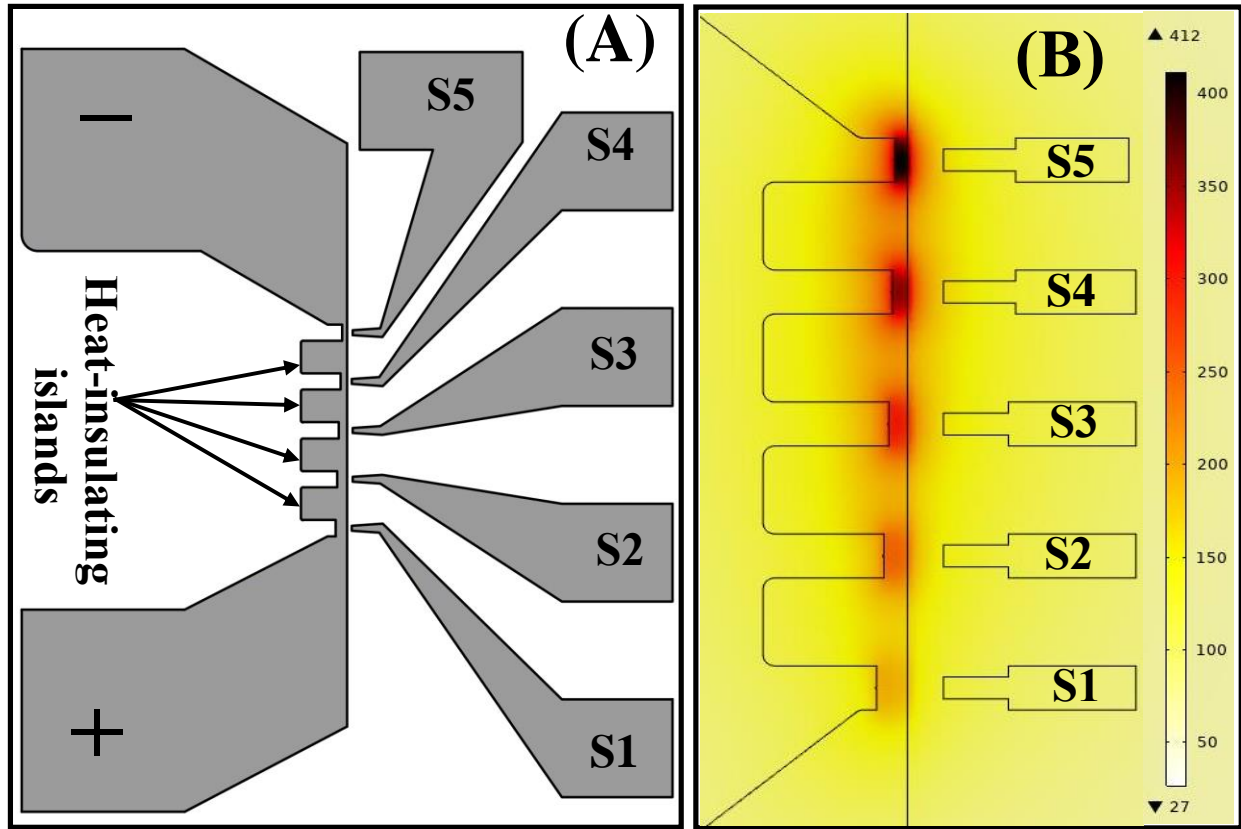
Figure 1. (A) Design and (B) simulation result of heat distribution of the five sensors

2.2 Fabrication of the sensor array

The sensor array fabrication process using conventional photolithography are shown in Figure 2. The steps for making the microheater and the electrodes include (1) spin coating of photoresist, (2) UV light exposure and development and (3) deposition of Pt/Cr and (4) lift-off. The steps of depositing sensing material include (5) to (8), which need no explanation. The thin film of the sensing material SnO_2 with a thickness of 50 nm was reactively sputtered from a Sn target in a

7

Ar/O$_2$ gas mixture environment [29]. A thin layer of Pt with a thickness of 2 nm was then

deposited in the same sputtering system, but in only Ar environment. The base pressure and that

during the sputtering were 10^{-6} and 10^{-3} torr, respectively. The sputtering power was fixed at 30

W for deposition of both SnO$_2$ and Pt. The thicknesses of SnO$_2$ and Pt were optimized to

maximize the sensor response, as reported in [30].
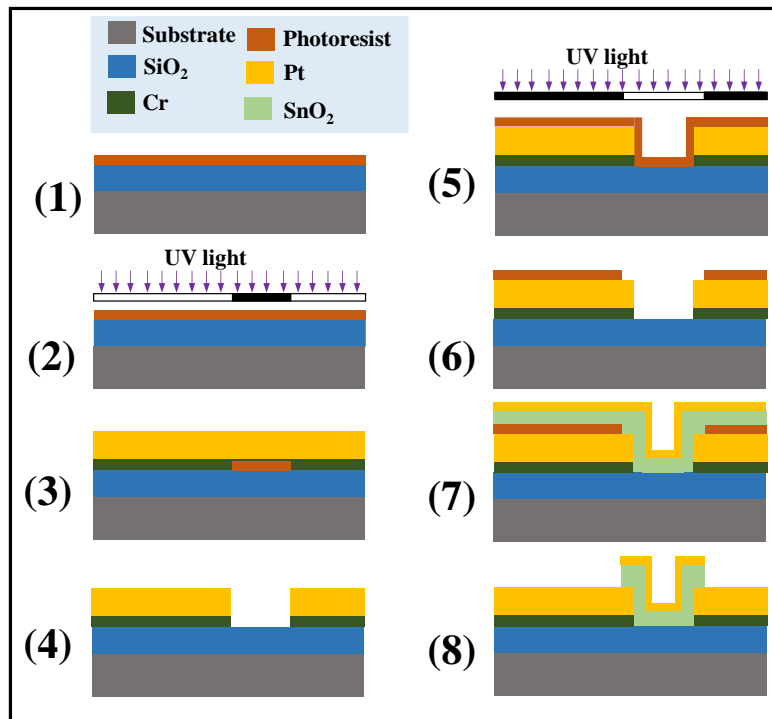
Figure 2. Process steps for fabrication of the sensor array

2.3 Sensor characterization

For easy and safe handling of the sensor chip a special PCB for mounting it was fabricated. The

PCB with the sensor chip then was connected to an electrical characterization system. The

transient output voltage from each sensor was measured on a reference resistor ($R_{ref.i}$) connected

in series with the sensor using a home-made data acquisition system (Figure S1, Supplementary).

Details about the data acquisition system can be found in [31]. By applying a voltage on the

8

microheater, the power consumed by the sensor array could be calculated as $P=V^2/R$, where V is the applied voltage and R is the resistance of the microheater. For the thermal test, powers of 30, 50, and 80 mW were applied and temperatures from each sensor were measured using an IR microscope (Thermovision A40, Flir system, USA), as shown in Figure 3. For the gas-sensing characterization, the atmosphere was switched from air to analytic gas and back to air while the output voltages from the five sensors were recorded by the data acquisition system and used to calculate the sensor responses. The sensor response of each sensor was defined as $S=V_{gas}/V_{air}$, where V_{gas} and V_{air} were the voltage drop across its reference resistor in analytic gas and in air, respectively. Six gases were tested in the present study, namely ammonia, hydrogen, methanol, acetone, ethanol, and isopropanol (IPA).

3. Results and discussion

Optical microscopy photos of the fabricated sensor array are shown in Figure 3(A) and (B). The inset in Figure 3(A) is a photo of two sensor chips compared with the tip of a ballpoint pen. The size of the sensor chip is 5×5 mm^2. Figure 3(B) shows the center part of a fabricated sensor chip. The five sensors were marked as S1, S2, S3, S4 and S5, consecutively. The inset in Figure 3(B) shows the sensing material of one sensor, with the size of approximately 6×15 µm. A SEM image of the Pt/SnO$_2$ thin film is shown in Figure 3(C). The thin film surface includes many grains smaller than 20 nm, which are not present on the very smooth surface of the bare SnO$_2$ thin film (inset in Figure 3(C)). Thus, the grains can be attributed to the aggregation of the thin Pt film formed during the thermal treatment. The cross-section SEM image of the Pt/SnO$_2$ thin film confirms its thickness of about 150 nm (Figure 3(D)). In this study, the thickness Pt is only about 2 nm, therefor it is difficult to distinguish the interface between the two layers in the cross-section SEM image. Nevertheless, XRD pattern of the Pt/SnO$_2$ thin film (Figure 3(E)) shows the

typical diffraction peaks of tetragonal SnO_2 (JCPDS No. 41-1445) and cubic Pt (JCPDS No. 65-2868) [32]. The decoration with metallic Pt on the surface of the SnO_2 thin film is very important for enhancing the gas sensing properties, for example toward hydrogen [33]. Notably, the intensity of the Pt peaks is relatively high because the Pt layer was deposited on top of the SnO_2 thin film. The SnO_2 diffraction peaks are very broad, indicating the nanocrystallinity of the fabricated thin film [34]. The average crystal size calculated by Scherrer equation using the (110) peak of SnO_2 is about 12 nm. The crystal size of SnO_2 is about twice its Debye length (~3.36 nm) at operation temperature of about 250 °C, ensuring the high gas responsivity [35]. Compared with the SnO_2 thin film sensor sensitized with microsized Pd islands in [34], the bilayer Pt/SnO_2 thin film has the advantage that it avoids the use of one mask in the fabrication process. EDS analysis of the Pt/SnO_2 thin film shown in Figure 3(F) confirms the presence of O, Sn, Pt elements. The peak of Si element in the EDS analysis comes from the silicon substrate. The elemental composition of different elements is 54.16, 44.60, 0.92 and 0.32 atom% for O, Si, Sn, and Pt, respectively. Since the content of Si and O comes from the substrate, the Pt/SnO_2 thin film composition estimated by EDS analysis is not expected to be quantitatively accurate.
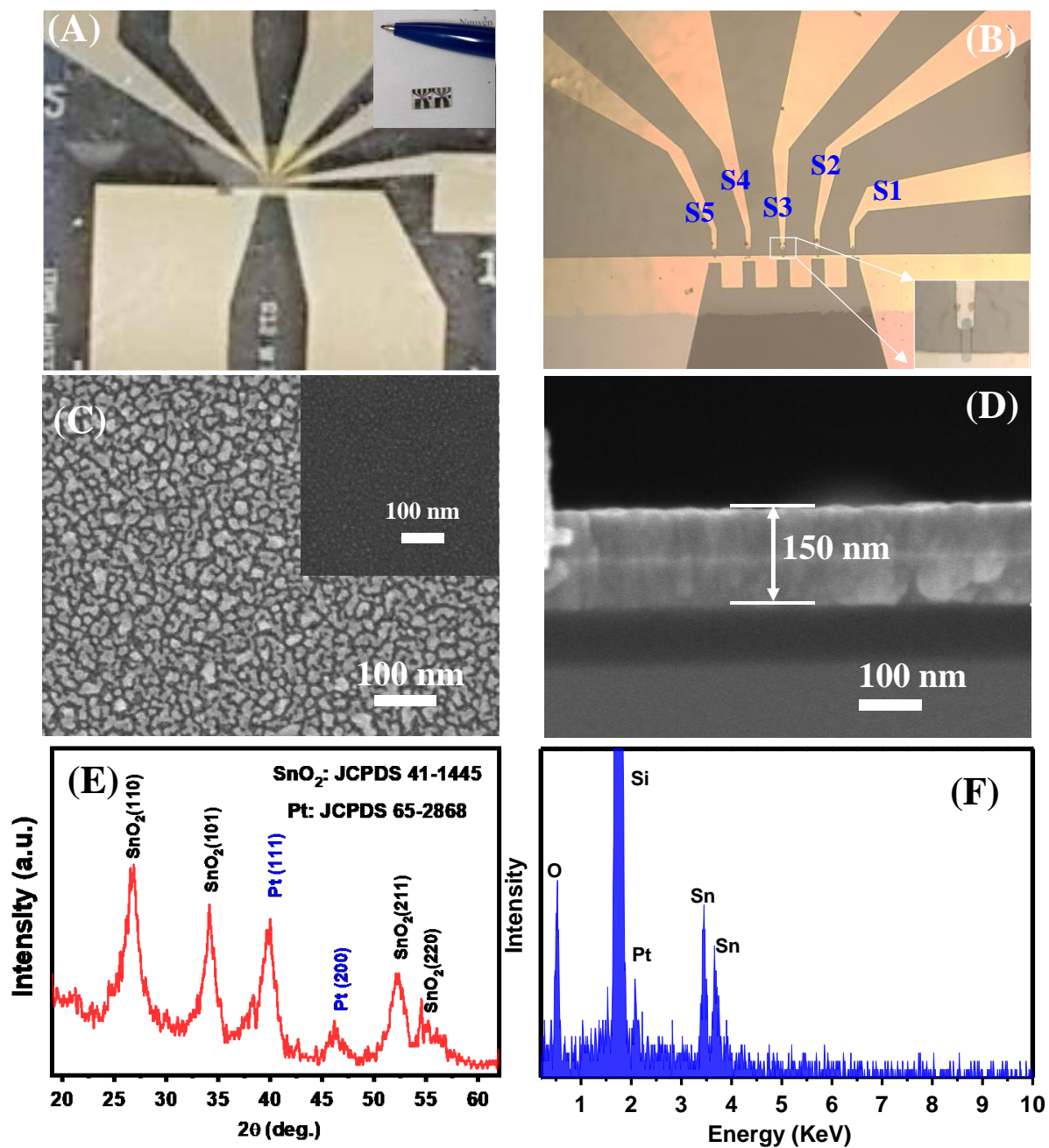
Figure 3. (A) Optical microscopy image of the sensor chip. The inset shows two chips compared with the tip of a ballpoint pen; (B) Optical microscopy image of the center part of the chip; (C) Top-view SEM image of the Pt-decorated SnO_2 thin film. The inset shows a top-view SEM of the bare SnO_2 film; (D) SEM image of the cross-section of the 150 nm SnO_2 and 2 nm Pt; (E) XRD pattern of the Pt/SnO_2 thin film; and (D) EDS analysis of the Pt/SnO_2 thin film.

1   The Pt/SnO$_2$ thin film was further studied by XPS analysis, as shown in Figure 4. The survey

2   scan of the thin film shown in Figure 4(A) reveals the presence of Sn, O, C and Pt, which is in

3   consistency with the XPS database of SnO$_2$ and Pt. The atomic composition of the sample

4   calculated form the XPS data is 42.4, 26.8, 23.2, 5.2 and 2.5% for O, Sn, C, Pt and N,

5   respectively. An atomic ratio of [O]/[Sn]=1.58 is obtained, which confirms that the deposited

6   SnO$_2$ is nonstoichiometric. The C1s peak of contamination carbon at 284.8 eV is used as the

7   reference for other XPS peaks. Figure 4(B) is a high resolution scan of the Sn3d, which shows

8   two peaks at 495.04 and 486.6 eV, attributed to the binding energies of Sn3d$_{3/2}$, and Sn3d$_{5/2}$,

9   respectively. The binding energies of Sn3d$_{3/2}$ and Sn3d$_{5/2}$ peaks here are in consistency with

10   those of Sn^{4+} species, confirming the formation of SnO$_2$ in the thin film. The difference of the

11   two binding energy peaks of Sn3d$_{3/2}$ and Sn3d$_{5/2}$ is 8.44 eV, in agreement with the reported

12   literature, confirming the oxidation state of Sn(IV) [36]. The core-levels of Pt4f were also

13   studied by high resolution XPS scan as shown in Figure 4(C). The two peaks with binding

14   energies of 71.24 and 74.56 eV are attributed to Pt4f$_{7/2}$ and Pt4f$_{5/2}$ of Pt^0, respectively [37,38].

15   The results confirm that the Pt deposited on the surface of the SnO$_2$ thin film is in metallic and

16   not oxide form. The presence of metallic Pt is desired for enhancement of the gas sensing

17   performance due to the higher catalytic activity compared with the Pt oxide forms [36].

18
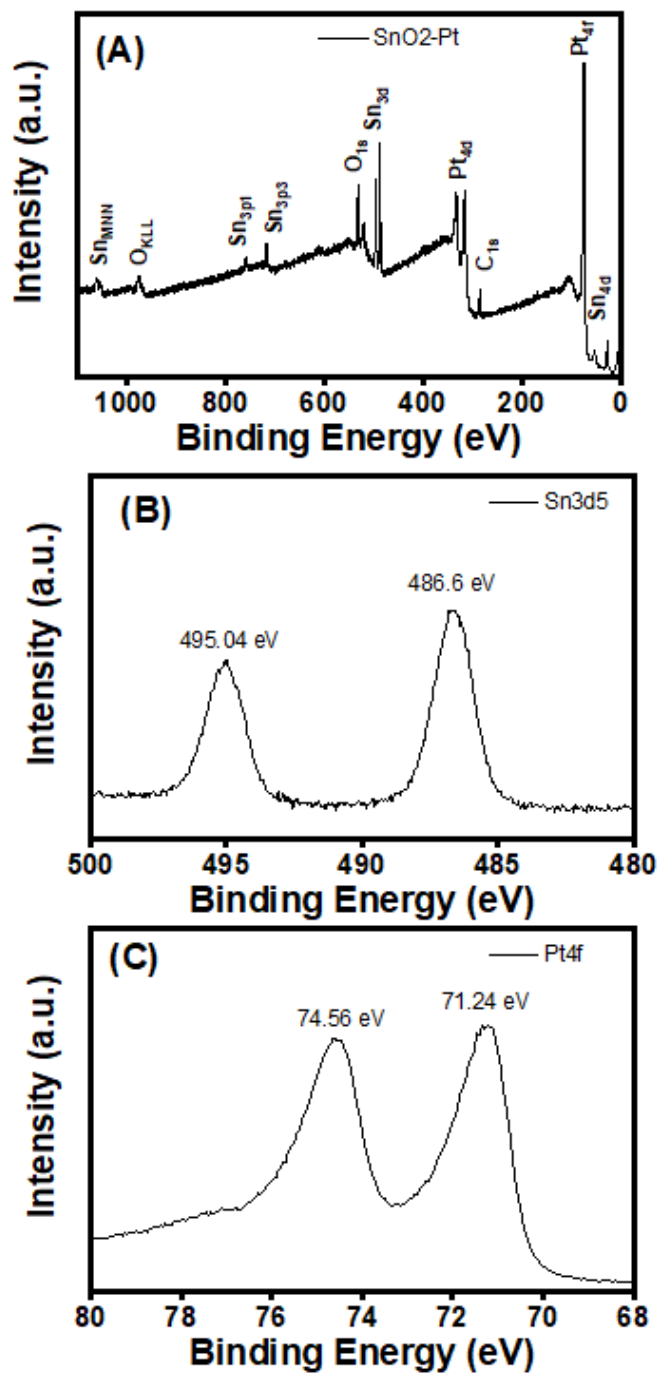
Figure 4. XPS analysis of the SnO$_2$/Pt thin film: (A) survey scan; high-resolution scan of core-levels (B) Sn3d; and (C) Pt4f.

1   Before testing the gas sensing performance of the sensor array, the temperature gradients from

2   the micro heater at different applied powers was tested. As shown in Figure 5(A), (B) and (C),

3   the infrared microscopy photos of the chip at applied powers of 30, 50, and 80 mW display the

4   actual temperature gradients with interval of about 50 °C. Notably, in the metal oxide

5   semiconductor based gas sensor, the device exhibits clearly different response trends with step of

6   temperature gradient of about 50 °C [19]. The temperature plots of the S1–S5 sensors at applied

7   powers of 30, 50 and 80 mW shown in Figure 5(D) document the actual temperature gradient

8   from 69 to 398 °C. The results suggest that by using a single chip with five sensors and three

9   applied powers, 15 data series of sensing signals in a single measurement can be generated. Of

10   course the number of sensors and their simultaneous signals can be higher, as reported in the

11   literature, for example ten sensors were used in a measurement system to classify gases via deep

12   machine learning [39]. Here, the applied power is limited to 80 mW to prevent damage of the

13   sensor and ensure its durability. As shown in Figure S2 (Supplementary), when a total power of

14   90 mW is applied for 15 minutes, the S5 sensor heater is broken, making the whole sensor array

15   unusable since the microheater segments are arranged in series. With the highest applied power

16   of 80 mW, the temperatures of sensors S1, S2, S3, S4 and S5 are 190, 241, 293, 345 and 398 °C,

17   respectively. The resulting temperature gradient is appropriate to make the five sensors behaving

18   differently, as discussed latter.
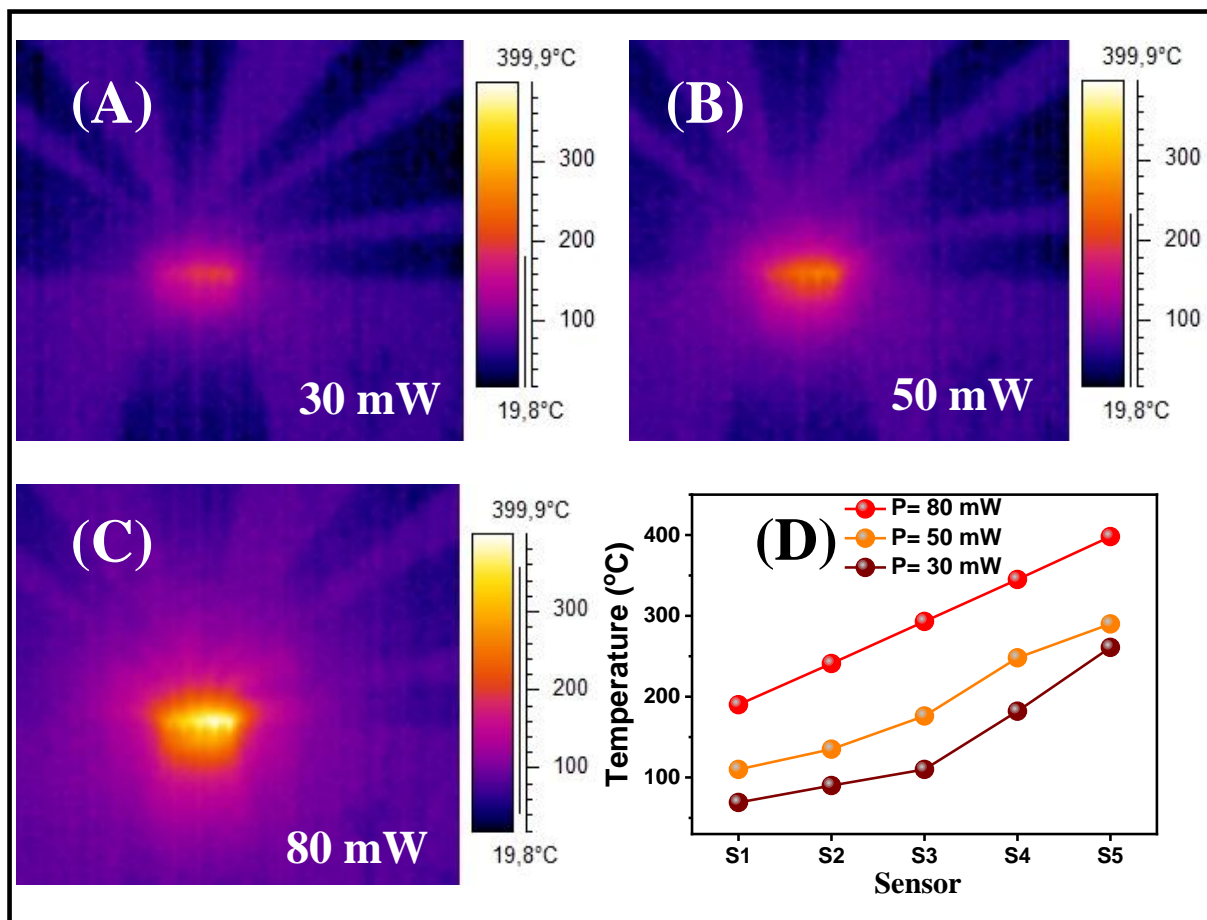
Figure 5. IR images at (A) P = 30 mW; (B) P = 50 mW; (C) P = 80 mW; and (D) temperatures of the five sensors at different powers

To evaluate the sensing performance of the sensor array, the response characteristics of the five sensors to hydrogen at a power of 80 mW were first tested. Figure 6(A) shows the transient response-recovery characteristics when periodically exposing the sensors to different H_2 concentrations from 25 to 250 ppm. The response values S of all sensors increased significantly with the increase of the H_2 concentration. The increase of the responses against H_2 gas confirms that the Pt/SnO$_2$ thin film has the n-type semiconducting characteristics [40]. For all five sensors, the responses increase with the increase of H_2 gas concentrations over the measured range, indicating the non-saturation of the sensor and thus capability of effective application in

monitoring H_2 at wide range concentration. It is clear that at each H_2 concentration, the response

and recovery characteristics improved from sensor S1 to sensor S5. This can be explained by the

temperature increase from sensor S1 to sensor S5, accordingly. The responses of the five sensors

to various H_2 concentrations are shown in Figure 6(B). The sensor S2 has the highest response

value to H_2 at all concentrations when applying the power of 80 mW, suggesting that the

temperature of this sensor, of around 241°C, is the optimal working temperature. The response

values of this sensor were 2.1, 3.4, 4.5 and 8.2 at 25, 50, 100 and 250 ppm H_2, respectively. The

responses of this sensor, as shown in Figure S3 (Supplementary), increase almost linearly with

the H_2 concentrations in the measured range, which is an advantage for the actual application in

designing a sensor instrument [41,42].

To correlate the exact temperature of each sensor in the array, the hydrogen sensing

characteristics of the sensor S2 was tested by using an external heater that generated

temperatures from 50 to 350 °C with a step of 50 °C against the same H_2 concentrations as

before (25–250 ppm). It was interesting to see that the sensor S2 showed superior sensitivity

when using external heater compared with that when using the built-in microheater, as shown in

Figure 6(C). The sensor S2 exhibited the maximum response value of XXX at a working

temperature of 200°C, compared with the maximum response value of YYY at 241 °C when

using the built-in microheater at the applied power of 80 mW and measuring with the IR

microscope. Notably, this temperature value is much lower than that in the other reports on H_2

sensors based on SnO_2 disks [43] or Pt-SnO_2 nanoparticles [10.1016/j.jallcom.2019.07.081]. In

addition, the fabricated sensor also exhibited superior sensitivity if it is noted that a gas sensor

based on a Pd thin film exhibited a low response value of 4% to 4000 ppm of H_2 at 400°C [44].

The higher response values of the sensor S2 when using the external heater and exposing to the

1   same range of gas concentration can be explained by the fact that the thermal energy of the

2   external heater (actually a hot plate) is sufficient to pre-activate the gas in the sensor ambient

3   trigging it to react with the pre-absorbed oxygen species.

4   The repeatability of the sensor performance is important for any application; therefore the short-

5   term stability of the sensor was tested during six consecutive exposures to H_2 and back to air, as

6   shown in Figure 6(D). As seen here, the sensor array exhibited good repeatability without any

7   significant change in the response values.
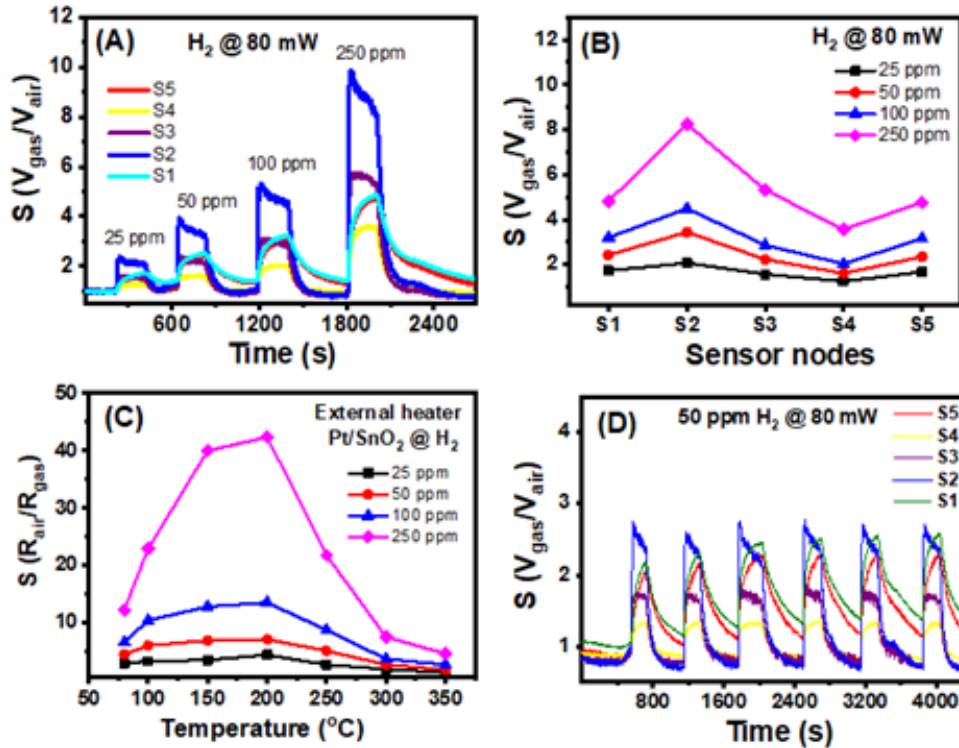
8

9   **Figure 6.** (A) Transient response-recovery characteristics to periodic exposure to H_2 (25–250

10   ppm) at the power of 80 mW; (B) correspondent sensor response; (C) sensor response measured

11   at different temperatures using an external heater; (D) repeatability of the five sensors on the

12   detection of 50 ppm of H_2 at 80 mW.

17

The gas sensing characteristics of the sensor array at the applied power of 80 mW were tested then against various gases, including ammonia (NH_3), methanol, acetone, ethanol and iso-propanol (IPA). The transient response-recovery characteristics of the fabricated sensors to the gases are shown in Figure 7(A–E). Figure 7(A) shows the dynamic responses of the five sensors to NH_3 with concentrations of 20, 50, 100, and 250 ppm. Like for H_2, the response values here also increase as the concentration of the test gas increases. For a given NH_3 concentration the response value was different for each sensor. The response plots of the five sensors to different NH_3 concentrations are shown in Figure 7(F). The sensor S2 has the highest response value compared with the others sensors at all gas concentrations, confirming that 241°C is also the optimal working temperature for detection of NH_3. The response values of the sensor S2 are 9.2, 14.9, 27.1 and 44.3 at 25, 50, 100 and 250 ppm NH_3, respectively. These results demonstrate that the microheater designed for the five sensors is effective for covering an adequate working temperature range. Similar response characteristics of the sensors were obtained when tested against methanol, acetone, ethanol and IPA (Figure 7(B–E) and (G–K)). Sensor S2, again, showed the highest response value among the five sensors to all tested gases, with an exception of acetone, to which the S3 sensor exhibited the highest response. This means that the optimal working temperature for detection of acetone is 293 °C. The responses of the five sensors (right column of Fig. 7) show clearly that the trend is different for each gas, and this demonstrates that the sensor array design is effective for classification of the tested gases. Notably, in this sensor array design, heat sinks are used between the microheater segments so that each sensor has its own heat source arranged in the desired temperature gradient. Compared with the sensor array designed with a single heat source in a previous report [31], the design in this work is better in respect of easy determining positions of the sensors and distances between them.
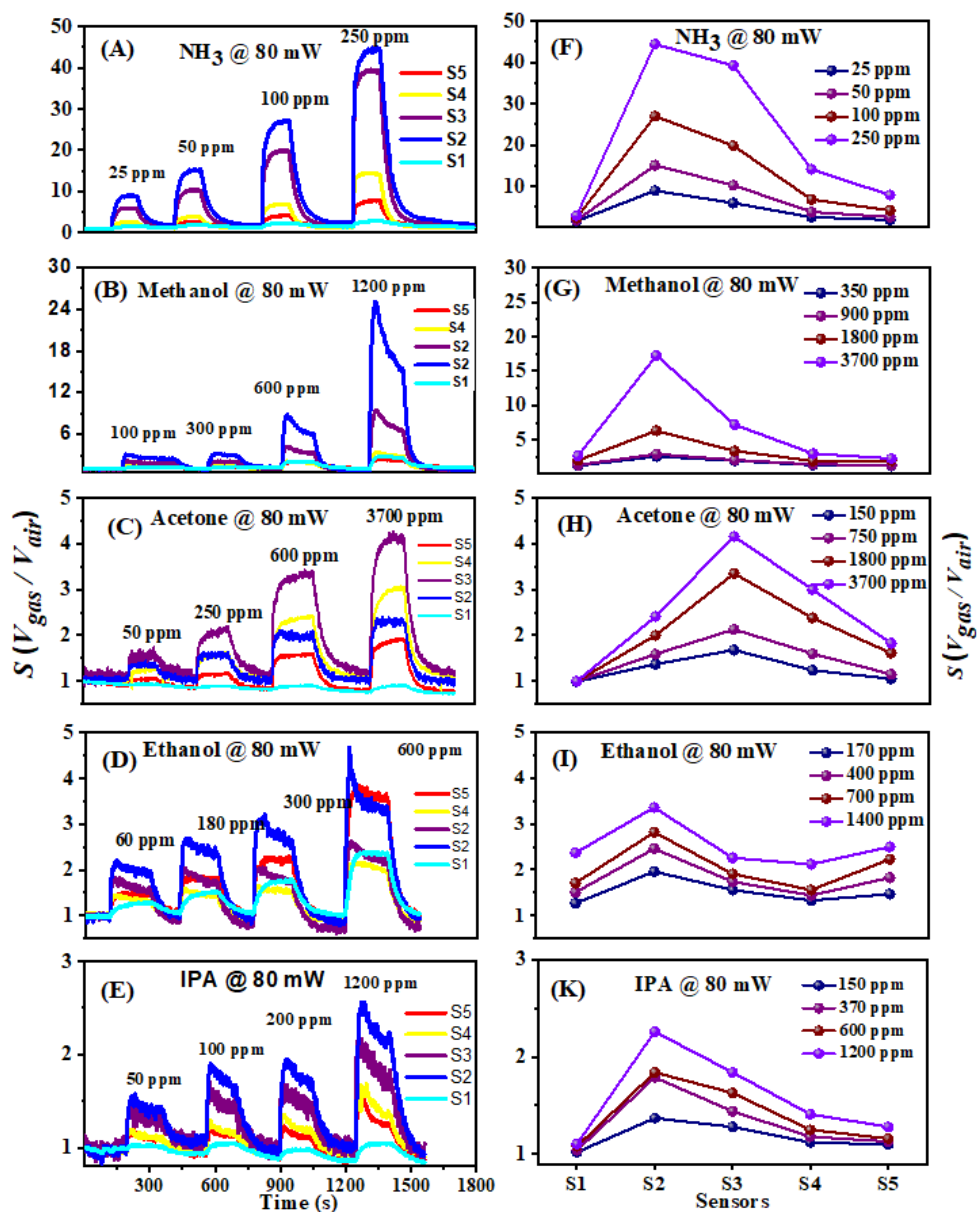
Figure 7. Gas sensing characteristics of the sensors S1–S5 at the applied power of 80 mW: transient response-recovery characteristics upon periodic exposure of (A) NH$_3$, (B) Methanol, (C) Acetone, (D) Ethanol and (E) Iso-propanol; and plots of responses (S) to different concentrations of (F) NH$_3$, (G) Methanol, (H) Acetone, (I) Ethanol and (K) Iso-propanol

1   The so called radar plot is effective for classification of different gases using an array of sensors

2   [45]. In this study, the five sensors are fabricated in the same process steps with the same

3   SnO2/Pt sensing material. They are arranged in such an array that allows them to work at

4   different pre-determined temperatures. This design enables the sensor to respond selectively to

5   different gases. The radar plot showing their selectivity is presented in Figure 8 (A). The shape

6   and size of the graphs are different for each gas, confirming the capability of the sensor array to

7   be used for classification of different gases. Notably, the size and shape of the radar plots for

8   sensing methanol, hydrogen and ammonia here are very different, and the concentration of

9   hydrogen, ammonia and ethanol is much lower than that of the other gases. However, the plots

10   are different and distinguishable for the six gases. It is worthwhile to know that in the study

11   reported by Lee et al. [46], an array of 3x3 sensors based on WO_3, SnO_2, and NiO decorated with

12   Au nanoparticles was used for the detection and classification of acetone, toluene, ammonia and

13   hydrogen sulfide by principal component analysis, where the temperature was varied to 150, 200,

14   250, and 300 ^{o}C. To highlight the relationships between the sensing results of the gases, the

15   principal component analysis (PCA) method is also used here, as shown in Figure 8(B). The

16   clear positions and distances that separate the groups of points relating to the individual gases

17   strengthen the classification results in the radar plots, namely ammonia is the most

18   distinguishable, followed by H_2 and methanol. Acetone, ethanol and IPA, although

19   distinguishable, are more similar to each other.

20
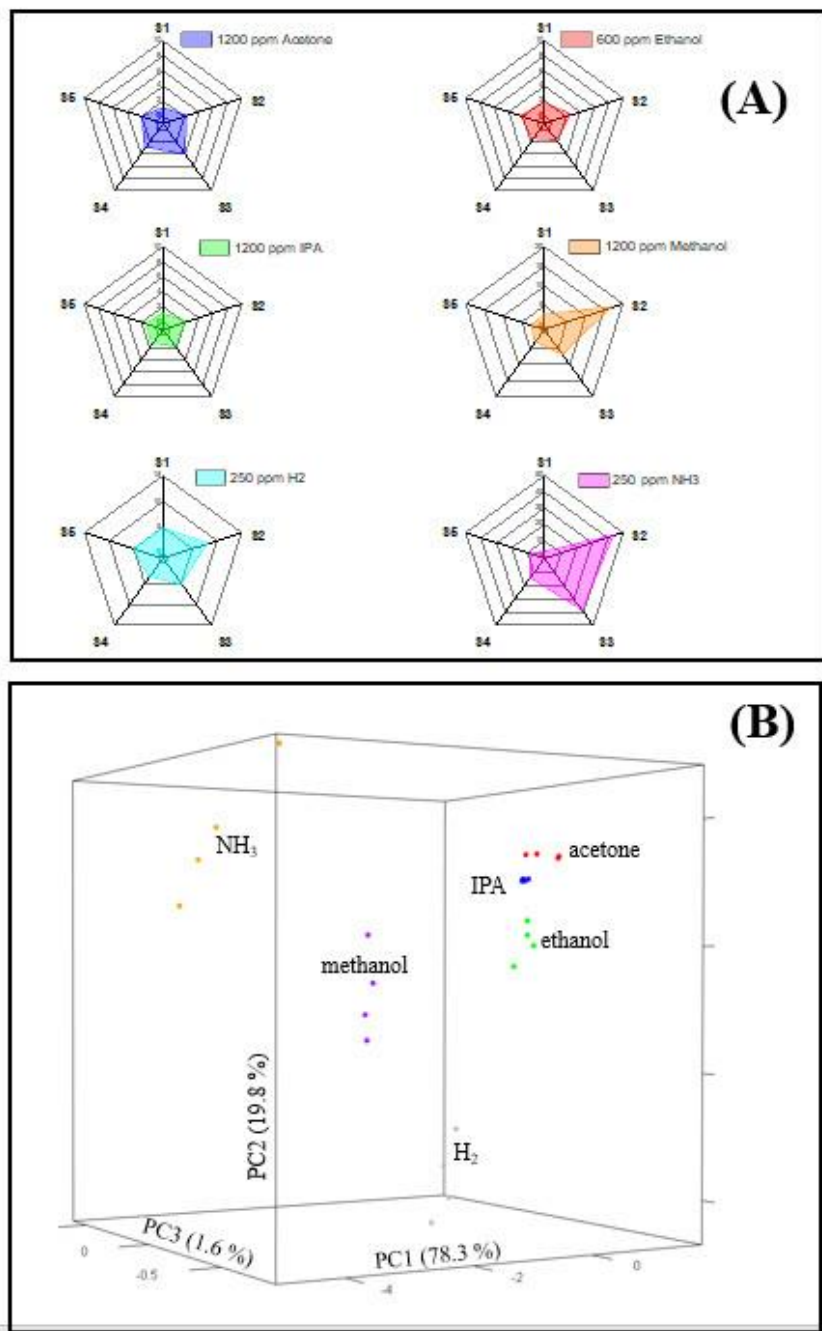
Figure 8. (A) Radar plot for the six tested gases (methanol, IPA, ethanol, NH_3, H_2S, H_2) at the applied power of 80 mW, and (B) gas classification by PCA method

4. Conclusion

A design and fabrication of SnO_2/Pt thin film sensor array for effective detection and classification of multiple gases was presented. The sensor array consisting of five sensors on a chip was simulated by using COMSOL Multiphysics to obtain the desired temperature gradient and the chip was fabricated by using conventional photolithography, deposition and lift-off technique. The microheater and the five sensor electrodes of Pt/Cr thin films were fabricated simultaneously in the same process, followed by deposition of the same sensing material of SnO_2/Pt thin films for the five sensors. The identical sensors were arranged in a temperature gradient of 190, 241, 293, 345 and 398 °C at an applied power of 80 mW. By using radar plots and the PCA, it was possible to analyze the measurement data from the five sensors to classify different gases. The developed sensor array with small size, high rapidity, stability, portability, and robustness demonstred its strong dandidacy to using in real gas measurement instruments and electronic noses.

References

[1]   L. Van Duy, N. Van Duy, C.M. Hung, N.D. Hoa, N.Q. Dich, Urea mediated synthesis and acetone-sensing properties of ultrathin porous ZnO nanoplates, Mater. Today Commun. 25 (2020) 101445. doi:10.1016/j.mtcomm.2020.101445.

[2]   R.A. Potyrailo, S. Go, D. Sexton, X. Li, N. Alkadi, A. Kolmakov, B. Amm, R. St-Pierre, B. Scherer, M. Nayeri, G. Wu, C. Collazo-Davila, D. Forman, C. Calvert, C. Mack, P. McConnell, Extraordinary performance of semiconducting metal oxide gas sensors using dielectric excitation, Nat. Electron. 3 (2020) 280–289. doi:10.1038/s41928-020-0402-3.

[3]   G.W. Hunter, S. Akbar, S. Bhansali, M. Daniele, P.D. Erb, K. Johnson, C.-C. Liu, D. Miller, O. Oralkan, P.J. Hesketh, P. Manickam, R.L. Vander Wal, Editors' Choice—Critical Review—A Critical Review of Solid State Gas Sensors, J. Electrochem. Soc. 167 (2020) 37570. doi:10.1149/1945-7111/ab729c.

[4]   C.M. Hung, D.Q. Dat, N. Van Duy, V. Van Quang, N. Van Toan, N. Van Hieu, N.D. Hoa, Facile synthesis of ultrafine rGO/WO3 nanowire nanocomposites for highly sensitive toxic NH3 gas sensors, Mater. Res. Bull. 125 (2020) 110810. doi:10.1016/j.materresbull.2020.110810.

[5]   N.H. Hanh, L. Van Duy, C.M. Hung, N. Van Duy, Y.-W. Heo, N. Van Hieu, N.D. Hoa, VOC gas sensor based on hollow cubic assembled nanocrystal Zn2SnO4 for breath analysis, Sensors Actuators A Phys. 302 (2020) 111834. doi:10.1016/j.sna.2020.111834.

[6]   J.-W. Yoon, J.-H. Lee, Toward breath analysis on a chip for disease diagnosis using semiconductor-based chemiresistors: recent progress and future perspectives, Lab Chip. 17 (2017) 3537–3557. doi:10.1039/C7LC00810D.

[7]   S. Su, J. Hu, Gas Identification by a Single Metal-Oxide-Semiconductor Sensor Assisted by Ultrasound, ACS Sensors. 4 (2019) 2491–2496. doi:10.1021/acssensors.9b01113.

[8]   D. Karakaya, O. Ulucan, M. Turkan, Electronic Nose and Its Applications: A Survey, Int. J. Autom. Comput. 17 (2020) 179–209. doi:10.1007/s11633-019-1212-9.

[9]   J. van den Broek, D. Bischof, N. Derron, S. Abegg, P.A. Gerber, A.T. Güntner, S.E. Pratsinis, Screening Methanol Poisoning with a Portable Breath Detector, Anal. Chem. 93 (2021) 1170–1178. doi:10.1021/acs.analchem.0c04230.

[10] R. Fend, A.H.J. Kolk, C. Bessant, P. Buijtels, P.R. Klatser, A.C. Woodman, Prospects for Clinical Application of Electronic-Nose Technology to Early Detection of Mycobacterium tuberculosis in Culture and Sputum, J. Clin. Microbiol. 44 (2006) 2039–2045. doi:10.1128/JCM.01591-05.

[11] Y. Zhang, J. Zhao, T. Du, Z. Zhu, J. Zhang, Q. Liu, A gas sensor array for the simultaneous detection of multiple VOCs, Sci. Rep. 7 (2017) 1960. doi:10.1038/s41598-017-02150-z.

[12] Z. Chen, Z. Chen, Z. Song, W. Ye, Z. Fan, Smart gas sensor arrays powered by artificial intelligence, J. Semicond. 40 (2019) 111601. doi:10.1088/1674-4926/40/11/111601.

[13] A.T. Güntner, V. Koren, K. Chikkadi, M. Righettoni, S.E. Pratsinis, E-Nose Sensing of

Low-ppb Formaldehyde in Gas Mixtures at High Relative Humidity for Breath Screening of Lung Cancer?, ACS Sensors. 1 (2016) 528–535. doi:10.1021/acssensors.6b00008.

[14] J. Zhang, Y. Xue, Q. Sun, T. Zhang, Y. Chen, W. Yu, Y. Xiong, X. Wei, G. Yu, H. Wan, P. Wang, A miniaturized electronic nose with artificial neural network for anti-interference detection of mixed indoor hazardous gases, Sensors Actuators B Chem. 326 (2021) 128822. doi:10.1016/j.snb.2020.128822.

[15] W. Li, H. Liu, D. Xie, Z. He, X. Pi, Lung Cancer Screening Based on Type-different Sensor Arrays, Sci. Rep. 7 (2017) 1969. doi:10.1038/s41598-017-02154-9.

[16] D. Drix, M. Schmuker, Resolving Fast Gas Transients with Metal Oxide Sensors, ACS Sensors. 6 (2021) 688–692. doi:10.1021/acssensors.0c02006.

[17] D. Feng, L. Du, X. Xing, C. Wang, J. Chen, Z. Zhu, Y. Tian, D. Yang, Highly Sensitive and Selective NiO/WO 3 Composite Nanoparticles in Detecting H 2 S Biomarker of Halitosis, ACS Sensors. 6 (2021) 733–741. doi:10.1021/acssensors.0c01280.

[18] G. Sakai, N. Matsunaga, K. Shimanoe, N. Yamazoe, Theory of gas-diffusion controlled sensitivity for thin film semiconductor gas sensor, Sensors Actuators B Chem. 80 (2001) 125–131. doi:10.1016/S0925-4005(01)00890-5.

[19] N. Bârsan, A. Tomescu, The temperature dependence of the response of SnO2-based gas sensing layers to O2, CH4 and CO, Sensors Actuators B Chem. 26 (1995) 45–48. doi:10.1016/0925-4005(94)01553-T.

[20] V. V. Sysoev, E. Strelcov, M. Sommer, M. Bruns, I. Kiselev, W. Habicht, S. Kar, L. Gregoratti, M. Kiskinova, A. Kolmakov, Single-Nanobelt Electronic Nose: Engineering and Tests of the Simplest Analytical Element, ACS Nano. 4 (2010) 4487–4494. doi:10.1021/nn100435h.

[21] M. Tonezzer, J.-H. Kim, J.-H. Lee, S. Iannotta, S.S. Kim, Predictive gas sensor based on thermal fingerprints from Pt-SnO2 nanowires, Sensors Actuators B Chem. 281 (2019) 670–678. doi:10.1016/j.snb.2018.10.102.

[22] J.M. Baik, M. Zielke, M.H. Kim, K.L. Turner, A.M. Wodtke, M. Moskovits, Tin-Oxide-Nanowire-Based Electronic Nose Using Heterogeneous Catalysis as a Functionalization Strategy, ACS Nano. 4 (2010) 3117–3122. doi:10.1021/nn100394a.

[23] C. Wongchoosuk, K. Subannajui, C. Wang, Y. Yang, F. Güder, T. Kerdcharoen, V. Cimalla, M. Zacharias, Electronic nose for toxic gas detection based on photostimulated core–shell nanowires, RSC Adv. 4 (2014) 35084–35088. doi:10.1039/C4RA06143H.

[24] V. Sysoev, I. Kiselev, M. Frietsch, J. Goschnick, Temperature Gradient Effect on Gas Discrimination Power of a Metal-Oxide Thin-Film Sensor Microarray, Sensors. 4 (2004) 37–46. doi:10.3390/s40400037.

[25] and A.K. Victor V. Sysoev, Joachim Goschnick, Thomas Schneider, Evghenii Strelcov, A Gradient Microarray Electronic Nose Based on Percolating SnO2 Nanowire Sensing Elements, Nano Lett. 2007, 7, 10, 3182–3188. (n.d.). doi:10.1021/nl071815+.

[26] S.Y. Park, Y. Kim, T. Kim, T.H. Eom, S.Y. Kim, H.W. Jang, Chemoresistive materials for electronic nose: Progress, perspectives, and challenges, InfoMat. 1 (2019) 289–316. doi:10.1002/inf2.12029.

[27] Y. Chen, M. Li, W. Yan, X. Zhuang, K.W. Ng, X. Cheng, Sensitive and Low-Power Metal Oxide Gas Sensors with a Low-Cost Microelectromechanical Heater, ACS Omega. 6 (2021) 1216–1222. doi:10.1021/acsomega.0c04340.

[28] P. Acuña-Avila, R. Calavia, E. Vigueras-Santiago, E. Llobet, Identification of Tequila with an Array of ZnO Thin Films: A Simple and Cost-Effective Method, Sensors. 17 (2017) 2943. doi:10.3390/s17122943.

[29] N. Van Toan, C.M. Hung, N. Van Duy, N.D. Hoa, D.T.T. Le, N. Van Hieu, Bilayer SnO2–WO3 nanofilms for enhanced NH3 gas sensing performance, Mater. Sci. Eng. B. 224 (2017) 163–170. doi:10.1016/j.mseb.2017.08.004.

[30] N.X. Thai, N. Van Duy, N. Van Toan, C.M. Hung, N. Van Hieu, N.D. Hoa, Effective monitoring and classification of hydrogen and ammonia gases with a bilayer Pt/SnO2 thin film sensor, Int. J. Hydrogen Energy. 45 (2020) 2418–2428. doi:10.1016/j.ijhydene.2019.11.072.

[31] N.X. Thai, N. Van Duy, C.M. Hung, H. Nguyen, M. Tonezzer, N. Van Hieu, N.D. Hoa, Prototype edge-grown nanowire sensor array for the real-time monitoring and classification of multiple gases, J. Sci. Adv. Mater. Devices. 5 (2020) 409–416. doi:10.1016/j.jsamd.2020.05.005.

[32] S. Chen, L. Shi, L. Wang, Mesoporous PtSnO2/C Catalyst with Enhanced Catalytic Activity for Ethanol Electro-oxidation, Kem. U Ind. 67 (2018) 19–27. doi:10.15255/KUI.2017.028.

[33] N. Van Duy, N.D. Hoa, N. Van Hieu, Effective hydrogen gas nanosensor based on bead-like nanowires of platinum-decorated tin oxide, Sensors Actuators B Chem. 173 (2012) 211–217. doi:10.1016/j.snb.2012.06.079.

[34] N. Van Toan, N. Viet Chien, N. Van Duy, H. Si Hong, H. Nguyen, N. Duc Hoa, N. Van Hieu, Fabrication of highly sensitive and selective H 2 gas sensor based on SnO 2 thin film sensitized with microsized Pd islands, J. Hazard. Mater. 301 (2016) 433–442. doi:10.1016/j.jhazmat.2015.09.013.

[35] N.D. Hoa, N. Van Quy, D. Kim, Nanowire structured SnOx–SWNT composites: High performance sensor for NOx detection, Sensors Actuators B Chem. 142 (2009) 253–259. doi:10.1016/j.snb.2009.07.053.

[36] L. Yang, X. Zhou, L. Song, Y. Wang, X. Wu, N. Han, Y. Chen, Noble Metal/Tin Dioxide Hierarchical Hollow Spheres for Low-Concentration Breath Methane Sensing, ACS Appl. Nano Mater. 1 (2018) 6327–6336. doi:10.1021/acsanm.8b01529.

[37] L.S. Kibis, D.A. Svintsitskiy, A.I. Stadnichenko, E.M. Slavinskaya, A. V. Romanenko, E.A. Fedorova, O.A. Stonkus, V.A. Svetlichnyi, E.D. Fakhrutdinova, M. Vorokhta, B.

Šmíd, D.E. Doronkin, V. Marchuk, J.-D. Grunwaldt, A.I. Boronin, In situ probing of Pt/TiO 2 activity in low-temperature ammonia oxidation, Catal. Sci. Technol. 11 (2021) 250–263. doi:10.1039/D0CY01533D.

[38] M. Liu, W. Tang, Z. Xie, H. Yu, H. Yin, Y. Xu, S. Zhao, S. Zhou, Design of Highly Efficient Pt-SnO 2 Hydrogenation Nanocatalysts using Pt@Sn Core–Shell Nanoparticles, ACS Catal. 7 (2017) 1583–1591. doi:10.1021/acscatal.6b03109.

[39] D. Ma, J. Gao, Z. Zhang, H. Zhao, Gas recognition method based on the deep learning model of sensor array response map, Sensors Actuators B Chem. 330 (2021) 129349. doi:10.1016/j.snb.2020.129349.

[40] J. Kang, J.-S. Park, H.-J. Lee, Pt-doped SnO2 thin film based micro gas sensors with high selectivity to toluene and HCHO, Sensors Actuators B Chem. 248 (2017) 1011–1016. doi:10.1016/j.snb.2017.03.010.

[41] N. Van Toan, C.M. Hung, N.D. Hoa, N. Van Duy, D. Thi Thanh Le, N. Thi Thu Hoa, N.N. Viet, P.H. Phuoc, N. Van Hieu, Enhanced NH3 and H2 gas sensing with H2S gas interference using multilayer SnO2/Pt/WO3 nanofilms, J. Hazard. Mater. 412 (2021) 125181. doi:10.1016/j.jhazmat.2021.125181.

[42] N.X. Thai, N. Van Duy, C.M. Hung, H. Nguyen, T.M. Hung, N. Van Hieu, N.D. Hoa, Realization of a portable H2S sensing instrument based on SnO2 nanowires, J. Sci. Adv. Mater. Devices. 5 (2020) 40–47. doi:10.1016/j.jsamd.2020.01.003.

[43] A. Umar, H.Y. Ammar, R. Kumar, T. Almas, A.A. Ibrahim, M.S. AlAssiri, M. Abaker, S. Baskoutas, Efficient H2 gas sensor based on 2D SnO2 disks: Experimental and theoretical studies, Int. J. Hydrogen Energy. 45 (2020) 26388–26401. doi:10.1016/j.ijhydene.2019.04.269.

[44] Q. Liu, J. Yao, Y. Wu, Y. Wang, G. Ding, Two operating modes of palladium film hydrogen sensor based on suspended micro hotplate, Int. J. Hydrogen Energy. 44 (2019) 11259–11265. doi:10.1016/j.ijhydene.2019.02.228.

[45] M. Abdelkhalek, S. Alfayad, F. Benouezdou, M.B. Fayek, L. Chassagne, Compact and Embedded Electronic Nose for Volatile and Non-Volatile Odor Classification for Robot Applications, IEEE Access. 7 (2019) 98267–98276. doi:10.1109/ACCESS.2019.2928875.

[46] J. Lee, Y. Jung, S.-H. Sung, G. Lee, J. Kim, J. Seong, Y.-S. Shim, S.C. Jun, S. Jeon, High-performance gas sensor array for indoor air quality monitoring: the role of Au nanoparticles on WO 3 , SnO 2 , and NiO-based gas sensors, J. Mater. Chem. A. 9 (2021) 1159–1167. doi:10.1039/D0TA08743B.

1